Sparse Aperiodic Optical Phased Arrays on Polymer Integration Platform

Adam Raptakis, Georgios Lymperakis, Lefteris Gounaridis, Madeleine Weigel, Moritz Kleinert, Christos Tsokos, Panos Groumas, Efstathios Andrianopoulos, Norbert Keil, Hercules Avramopoulos, *Member, IEEE*, and Christos Kouloumentas

***Abstract*— We demonstrate solid-state optical beam-steering utilizing polymer waveguides as edge emitters to form optical phased arrays (OPAs) for operation at 1550 nm. Waveguide spacing below the wavelength is hindered in low index contrast OPAs by cross-coupling, leading to the formation of unwanted grating lobes in the far field. We employ non-uniform spacing between the 16 channels of the OPAs to suppress the grating lobes and improve the unambiguous beam steering range. Three different aperiodic layouts are fabricated and experimentally tested. Within a steering range of ±10° we achieve an average beamwidth of 0.45° with an ordered spacing layout, and 0.52° and 0.69° with a randomized spacing layout of 8λ and 5λ average spacing, respectively. With the latter we show suppression of the sidelobes of >11 dB and >6 dB within a steering range of ±5° and ±8°, accordingly. Power consumption of 1.28 mW/π per channel is achieved thanks to the excellent thermo-optic (TO) coefficient of the polymer platform. To the best of our knowledge, we are the first to demonstrate polymer-based OPAs with aperiodic spacing.**

***Index Terms*— Integrated optics, phased arrays, optical polymers, beam steering, optical communications, remote sensing.**

I. Introduction

COMPACT solid-state beam scanners are essential for numerous emerging applications such as light detection and ranging (LiDAR), optical wireless communications (OWC), holographic displays, and biomedical imaging [1]. Optical phased arrays (OPAs), along with the maturation of photonic integration, open the way to realize cost-effective beam scanners with reduced size, weight, and power consumption. To steer an optical beam, OPAs use an array of coherent emitters to create constructive interference of the emitted light at certain angles in the far field by tuning the phase of each emitter. High scanning resolution over a wide field-of-view (FOV) requires large aperture arrays with closely spaced emitters. Increasing the spacing between emitters above λ/2, where λ is the wavelength, results in the formation of grating lobes, which render beam-steering outside a certain angle span ambiguous. However, positioning the emitters less than λ apart is challenging in photonic integrated circuits due to cross-coupling between adjacent waveguides [2]. Non-uniform arrays allow emitters to be positioned at wider spacings (multiple λ), while suppressing grating lobes by spreading their power over many sidelobes at different angles. Moreover, owing to their sparsity, non-uniform arrays can form large apertures with significantly fewer elements than uniform arrays, thus achieving the same beam divergence with lower complexity and power consumption [3], [4], [5], [6], [8].

Realizations of OPAs in silicon (Si) platforms have been the most prominent [1], [3], [4], [5], [6]. The high mode confinement and submicron dimensions of Si waveguides enable narrow waveguide spacing and thus a large scanning range. However, the same traits place restrictions on the handling of high optical powers due to the occurrence of nonlinear effects [7]. Silicon nitride (SiN) has been proposed as an alternative CMOS-compatible platform, more resilient to higher optical power due to its lower optical nonlinearity and larger core size, while its broad transparency makes it suitable for applications also in the visible region [8]. Nevertheless, phase tuning in most SiN-based OPAs has been relied so far on power-hungry thermo-optic (TO) phase shifters, posing scalability challenges.

Polymer-integrated optics technology, with its legacy in WDM optical communication systems and high-speed modulators, provides a mature platform with inherently high TO effect, strong thermal confinement, and high optical power handling capability [11]. The low thermal conductivity helps in reducing the power consumption of TO devices, although at the expense of lower tuning speeds. Beam scanners can benefit from the variety of devices that have been developed in the polymer platform such as high-efficiency tunable lasers, switches, and variable optical attenuators [12]. The fabrication of polymer devices, based on spin coating and UV lithography, offers a flexible and cost-effective manufacturing process that can support three-dimensional (3D) integration. Furthermore,

Manuscript received 8 December 2023; revised 30 January 2024; accepted 14 February 2024. Date of publication 20 February 2024; date of current version 8 March 2024. This work was supported by the European Commission through the Project H2020-ICT-3PEAT under Contract 780502. *(Corresponding author: Adam Raptakis.)*

Adam Raptakis, Georgios Lymperakis, Lefteris Gounaridis, Christos Tsokos, Efstathios Andrianopoulos, and Hercules Avramopoulos are with the Photonic Communications Research Laboratory, Institute of Communication and Computer Systems, National Technical University of Athens, 155 73 Zografou, Greece (e-mail: arap@mail.ntua.gr).

Madeleine Weigel, Moritz Kleinert, and Norbert Keil are with the Fraunhofer Institute for Telecommunications, HHI, 10587 Berlin, Germany (e-mail: moritz.kleinert@hhi.fraunhofer.de).

Panos Groumas and Christos Kouloumentas are with Optagon Photonics, 153 41 Agia Paraskevi, Greece, and also with the Photonic Communications Research Laboratory, Institute of Communication and Computer Systems, National Technical University of Athens, 155 73 Zografou, Greece (e-mail: christos.kouloumentas@optagon-photonics.eu).

Color versions of one or more figures in this letter are available at https://doi.org/10.1109/LPT.2024.3367973.

Digital Object Identifier 10.1109/LPT.2024.3367973

the electro-optic (EO) properties of polymer devices offer the possibility for ultra-high bandwidth modulation, although manufacturing challenges relevant to EO modulators are still to be resolved to support high-volume production [14].

In [17] a 32-channel polymer OPA was combined with a polymer-based tunable laser to demonstrate 2D scanning using an external diffraction grating. Leveraging on the 3D integration capability of polymer platforms, in [18] we proposed a multi-layer structure in Heinrich Hertz Institute's (HHI) PolyBoard integration platform, to form edge-emitting OPAs that can facilitate solid-state 2D beam-steering without the need for wavelength tuning. To prevent cross-coupling between the edge-emitting waveguides, a uniform spacing of 6 μm ($\sim$3.9λ) between the waveguides of the same layer was used, which limited the steering range to approximately $\pm 7°$ due to the presence of grating lobes. In the present work, we utilize aperiodic spacing to suppress grating lobes and improve on the scanning range. We realize three OPA chips using HHI's polymer-based integration platform PolyBoard, which contain different aperiodic layouts, and we experimentally characterize their performance.

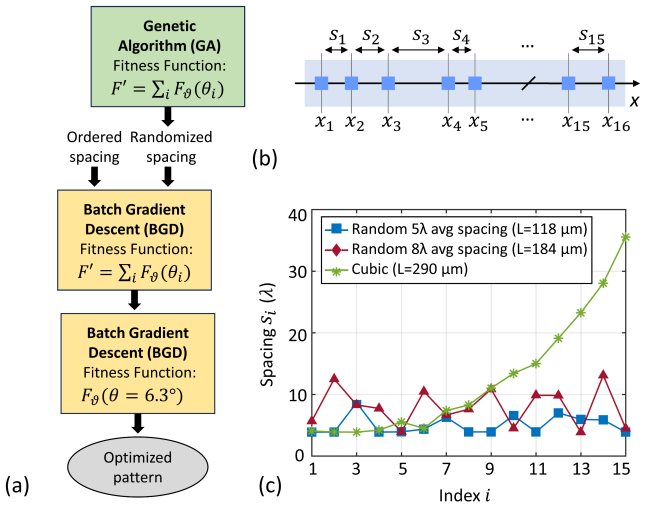

Fig. 1. (a) Flowchart of the optimization process used to design the aperiodic layouts. (B) Illustration of the emitting facet of the polyboard chip, Indicating the Non-Uniform Spacing Between the Edge-Emitting Waveguides. (C) spacing between the emitters for the three fabricated aperiodic layouts: random with average spacing 5λ and 8λ, and ordered spacing based on a cubic function.

II. Sparse Aperiodic Design

Two different methods are used to generate the non-uniform spacing between the 16 emitters: 1) ordered spacing based on a function (linear, quadratic, cubic etc.) and 2) random spacing using random offsets around a uniform grid [9]. In the case of randomized spacing we optimize the sidelobe suppression (SLS) in the range of interest (ROI) of the radiation pattern, i.e. [$-10°$, $10°$]. Various algorithms have been proposed to perform this task [5], [9], [10]. In our case a genetic algorithm (GA) is employed, while a batch gradient descent (BGD) algorithm is responsible for fine-tuning the spacing between the emitters in every layout. A commonly used fitness function is the SLS at a given target angle θ, noted here as $F_\vartheta(\theta)$. However, since this function only provides information for a specific target angle, it cannot capture the performance of the OPA in the entire ROI. For this reason, an additional fitness function F' was used, which is defined as the sum of the $F_\vartheta(\theta)$ for all target angles in ROI. To reduce the calculation time of F', only positive target angles are considered in the calculation since the radiation pattern is symmetrical around $0°$, hence, $F' = \sum_i F_\vartheta(\theta_i)$, $\theta_i \in [0, 10]$. The resolution of the θ_i vector can be configured according to the desired simulation time. In our case, we set a resolution of $0.1°$ resulting in a θ_i vector of 101 points in total.

The flow chart of the optimization procedure is presented in Fig. 1. The GA is employed with the fitness function F'. The population is set to 100 members, of which 20 members are mutated in each generation. Crossover is performed between the two best members of the population and a new member may only be included in the population if its fitness is above a certain threshold. The BGD algorithm optimizes F', and consequently $F_\vartheta(\theta_{3dB})$, where $\theta_{3dB} = 6.3°$ is the half-angle of the power of the single emitter. Optimization with $F_\vartheta(\theta_{3dB})$ can result in aperiodic layouts with smaller variations in SLS over a wider range of angles, which are generally better than patterns that exhibit higher SLS close to $0°$, but whose performance degrades dramatically at larger target angles. In each evaluation cycle the BGD algorithm shifts the position of each element on the array axis (x-axis) by the same random step (following a uniform distribution) either in the negative or in the positive direction and updates the position of the elements only at the end of the cycle, followed by a decrease of the maximum step by 0.99. The search loop runs for a total of 10^6 evaluation cycles and the best structure is saved. To calculate the intensity of the radiated far-field we use

$$\mathrm{I}_{FF}(\theta, \varphi = 0) = \mathrm{I}_0(\theta, \varphi) \left| \sum_{i=1}^{N} exp\left[jk_0 x_i \left(sin\theta - sin\theta_0 \right) \right] \right|^2 \tag{1}$$

where I_0 is the far-field radiation intensity of the individual emitter, k_0 is the wavenumber of the light in the vacuum, x_i is the position of the i-th emitter, and θ_0 is the target angle in the azimuthal (x-z) plane ($\varphi = 0$), in which the beam-steering takes place (see Fig. 2). The calculation of the radiation pattern for the 16 emitters is performed in $\sim$0.5 msec for 400 points, implemented in matrix operations in MATLAB.

Among the many aperiodic layouts that were generated with the above process, three were selected for fabrication, based on their SLS, main lobe power (MLP) and beamwidth. Fig. 1(c) shows the spacing between the emitters of the three patterns. Two of the layouts have random spacing with an average spacing of 5λ and 8λ, and the third layout has ordered spacing based on the cubic function. Their total size of the apertures is 118 μm, 184 μm, and 290 μm respectively. In the case of the ordered spacing in Fig. 1(c), the cubic function appears slightly changed due to the optimization with the BGD algorithm.

III. Experimental Results

The 16-channel aperiodic OPAs were designed and fabricated using the polymer-based platform of HHI based on

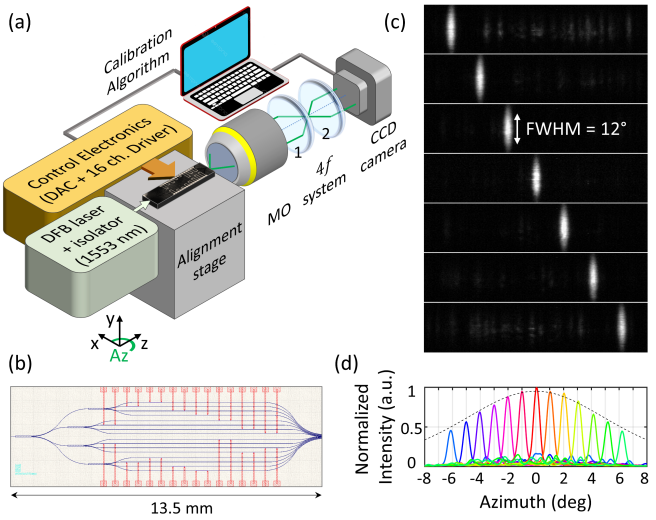

Fig. 2. (a) Measurement setup to characterize the far-field of the edge-emitting OPAs. (b) Photonic circuit of the 16-channel PolyBoard OPAs. The waveguide spacing at the east side of the chip vary on the design. (c) Normalized captured frames of the far-field from the CCD camera demonstrating scanning in the range ±6° with a step of 2°. (d) Cross section of frames showing measurements with an angle step of 1°. Measurements in (c) and (d) have been acquired with the randomized layout of 5λ average spacing OPA.

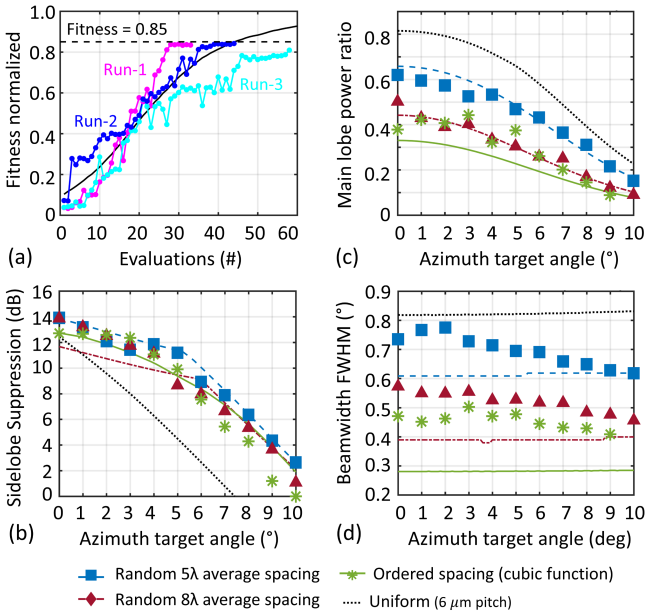

Fig. 3. (a) Experimental performance of the SPGD algorithm used for the calibration of the OPAs in three different runs. Measurements (markers) and theoretical curves (lines) of (b) SLS, (c) ratio of the main lobe power over the total radiated power, and (d) beam FWHM, for the three fabricated designs. The theoretical performance of a uniform array with 6 μm pitch is also plotted.

commercially available polymer materials (ZPU-12 series from ChemOptics Inc.) [11]. The cladding and core indices are 1.45 and 1.48 respectively at a wavelength of 1550 nm and provide a propagation loss of ~0.7 dB/cm. The core of the single-mode waveguide, serving as the edge-emitting element, has a square cross section of 3.2 μm × 3.2 μm. Due to the symmetry of the cross-section both TE and TM components of the single mode are equally supported. The optical power inserted to the chip is distributed among the 16 channels of the OPA by two stages of 1 × 4 MMI couplers. Heaters of 120 nm-thick Au on top of the waveguides are used for phase tuning, utilizing the high thermo-optic (TO) coefficient ($-1.1 \cdot 10^{-4}/K$) of the polymer platform. The average power for a π-phase change was measured to be $P_\pi = 1.28\ mW$, with heaters of 15 μm width and 500 μm length. Due to the low thermal conductivity of the polymer platform ($\sim 0.3\ W/m/K$) thermal crosstalk of less than 5% is expected for distances greater than 60 μm between adjacent waveguides, while even better isolation can be achieved by using air trenches [15]. The distance between adjacent channels in the phase tuning section of the chips is 180 μm. The waveguides were brought closer together on the emitting side of the chip to form the desired aperiodic layout. The dimensions of the chips are 7 mm × 13.5 mm.

To characterize the radiation pattern of the fabricated devices we use a standard camera setup (Fig.2 (a)): an NIR CCD camera, a microscope objective (MO) and a pair of lenses [18]. The latter forms a 4-f system that transfers the rear focal plane of the MO (i.e., the Fourier image) to the camera with a defined image ratio, enabling far-field measurement. To align the imaging system with the chip, lens-1 is removed so that the near-field (i.e., the real image) can be recorded. The chip is placed on a probe station with a passive heat sink. We use a fiber-pigtailed distributed feedback (DFB) laser at 1553 nm wavelength and a lensed fiber to couple 5 dBm of power into the chip. The initial OPA emission is random due to the fabrication error in the path lengths of the emitting waveguides. To extract the phase difference between the emitting waveguides, a stochastic parallel gradient-descent (SPGD) algorithm is used to converge the beam at 0° emission (along the z-axis), using feedback from the camera. We use Eq. (1) to steer the beam to the desirable azimuth angle, and the SPGD algorithm to further optimize the emission with respect to the SLS. Fig. 3(a) shows the number of evaluations required with our calibration algorithm to experimentally converge the beam at 0°. On average, 35 evaluations were sufficient to accurately determine the initial phases, corresponding to a maximum fitness of 0.85 (similarity with the theoretical radiation pattern). The time for each evaluation was set to approximately 1 second, primarily limited by the frame rate of the camera and control electronics, but further optimization is possible with the existing setup. The heating elements of our polymer platform can support tuning in the millisecond range (~2 ms).

Fig. 3(b)-(d) shows the measurement results from the characterization of the fabricated samples. We measured the SLS, the beam FWHM in the beam-steering plane and the MLP relative to the total radiated power within a scan range of ±10°. We indicate the measurements with markers and the corresponding theoretical values using lines. For conciseness, we fold the horizontal axis to show only the positive steering angles and record the average value between the measurement at the positive and negative target angles. Although the measurements were not completely symmetrical around 0°, their difference was less than 0.5%, 8% and 13%, for SLS, beamwidth and MLP ratio, respectively. For comparison, we also plot the corresponding SLS of the uniform layout

TABLE I
PERFORMANCE COMPARISON OF POLYMER-BASED OPAS

	[13]	[16]	[17]	[18]	**This work***
Array	8	16	32	2×4	**16**
Steering range	19.1°	7°	8.9°	10°×12°	**16°**
Beamwidth	3.9°	N.R.	0.7°	6°×2°	**0.69°**
Phase shifter	EO	TO	TO	TO	**TO**
P_π	~40 uW	2.5 mW	2 mW	N.R.	**1.28 mW**

* 5λ average spacing design

with 6 μm pitch. In Fig. 3(b) we see that the randomized layout with an average distance of 5λ has SLS of more than 11 dB up to a steering angle of 5°, while for the same FOV the cubic pattern has more than 8.7 dB. To calculate the total radiated power, we integrate the pixels over the entire frame captured by our imaging system. The best performing structure in terms of MLP is the layout with 5λ average spacing, due to its smaller aperture size (Fig. 3(c)). The average values of the measured beam FWHM were 0.69°, 0.52° and 0.45° for the 5λ and 8λ randomized layouts, and the ordered layout accordingly. Almost twice the number of channels (~30 channels) is needed to achieve 0.45° beamwidth with a 6 μm spacing uniform array [19]. The wider than optimal measured beamwidth shown in Fig. 3(d), may be due to the resolution of our imaging system (~0.05°/pix), in combination with the noise of the camera. Another factor may be the limitation of the algorithm to form a very sharp beam with the selected angular step ($\Delta\varphi = 15°$). A comparison of our 5λ average spacing design with recent work on polymer-based OPAs is show in Table I.

IV. CONCLUSION AND OUTLOOK

We have demonstrated 1D optical beam-steering with 16-channel OPAs in HHI's polymer-based platform. The effectiveness of the non-uniform spacing in suppressing grating lobes has been experimentally validated. Aperiodic emitter spacing was used to achieve SLS of >11 dB and >6 dB within a beam-steering range of ±5° and ±8°, respectively. The FOV is limited by the beam divergence of the edge-emitting waveguide. The latter can be slightly improved by modifying the waveguide cross-section or the refractive index contrast, although not without increasing the propagation loss of the platform. The phase tuning is based on thermo-optical (TO) phase shifters and has a phase tuning efficiency of 1.28 mW/π. Although the present work demonstrated aperiodicity in a single waveguide layer, the same concept can be used to improve the performance of multi-layer devices in the Poly-Board platform that perform 2D beam-steering without the need for wavelength tuning [18].

REFERENCES

[1] C. V. Poulton et al., "Long-range LiDAR and free-space data communication with high-performance optical phased arrays," *IEEE J. Sel. Topics Quantum Electron.*, vol. 25, no. 5, pp. 1–8, Sep. 2019.

[2] W. Song et al., "High-density waveguide superlattices with low crosstalk," *Nature Commun.*, vol. 6, no. 1, p. 7027, May 2015.

[3] D. Kwong, A. Hosseini, Y. Zhang, and R. T. Chen, "1 × 12 unequally spaced waveguide array for actively tuned optical phased array on a silicon nanomembrane," *Appl. Phys. Lett.*, vol. 99, no. 5, p. 3, Aug. 2011.

[4] D. N. Hutchison et al., "High-resolution aliasing-free optical beam steering," *Optica*, vol. 3, no. 8, p. 887, Aug. 2016.

[5] R. Fatemi, A. Khachaturian, and A. Hajimiri, "A nonuniform sparse 2-D large-FOV optical phased array with a low-power PWM drive," *IEEE J. Solid-State Circuits*, vol. 54, no. 5, pp. 1200–1215, May 2019.

[6] T. Fukui et al., "Non-redundant optical phased array," *Optica*, vol. 8, no. 10, p. 1350, Oct. 2021, doi: 10.1364/OPTICA.437453.

[7] J. Bass, H. Tran, W. Du, R. Soref, and S.-Q. Yu, "Impact of nonlinear effects in Si towards integrated microwave-photonic applications," *Opt. Exp.*, vol. 29, no. 19, p. 30844, Sep. 2021, doi: 10.1364/oe.433646.

[8] M. C. Shin et al., "Chip-scale blue light phased array," *Opt. Lett.*, vol. 45, no. 7, p. 1934, 2020, doi: 10.1364/ol.385201.

[9] T. Komljenovic, R. Helkey, L. Coldren, and J. E. Bowers, "Sparse aperiodic arrays for optical beam forming and LiDAR," *Opt. Exp.*, vol. 25, no. 3, p. 2511, Feb. 2017.

[10] M. G. Bray, D. H. Werner, D. W. Boeringer, and D. W. Machuga, "Optimization of thinned aperiodic linear phased arrays using genetic algorithms to reduce grating lobes during scanning," *IEEE Trans. Antennas Propag.*, vol. 50, no. 12, pp. 1732–1742, Dec. 2002.

[11] Z. Zhang and N. Keil, "Polymer photonic devices," in *Nanomaterials, Polymers, and Devices*, 1st ed., E. S. W. Kong, Ed. Hoboken, NJ, USA: Wiley, 2015, pp. 233–272, doi: 10.1002/9781118867204.ch9.

[12] Z. Zhang et al., "Hybrid photonic integration on a polymer platform," *Photonics*, vol. 2, no. 3, pp. 1005–1026, Sep. 2015, doi: 10.3390/photonics2031005.

[13] Y. Hirano et al., "High-speed optical-beam scanning by an optical phased array using electro-optic polymer waveguides," *IEEE Photon. J.*, vol. 12, no. 2, pp. 1–7, Apr. 2020.

[14] I. Taghavi et al., "Polymer modulators in silicon photonics: Review and projections," *Nanophotonics*, vol. 11, no. 17, pp. 3855–3871, Aug. 2022.

[15] A. Maese-Novo et al., "Thermally optimized variable optical attenuators on a polymer platform," *Appl. Opt.*, vol. 54, no. 3, p. 569, Jan. 2015.

[16] S.-M. Kim, T.-H. Park, C.-S. Im, S.-S. Lee, T. Kim, and M.-C. Oh, "Temporal response of polymer waveguide beam scanner with thermo-optic phase-modulator array," *Opt. Exp.*, vol. 28, no. 3, p. 3768, Feb. 2020, doi: 10.1364/oe.383514.

[17] S.-M. Kim, E.-S. Lee, K.-W. Chun, J. Jin, and M.-C. Oh, "Compact solid-state optical phased array beam scanners based on polymeric photonic integrated circuits," *Sci. Rep.*, vol. 11, no. 1, p. 10576, May 2021, doi: 10.1038/s41598-021-90120-x.

[18] A. Raptakis et al., "2D optical phased arrays for laser beam steering based on 3D polymer photonic integrated circuits," *J. Lightw. Technol.*, vol. 39, no. 20, pp. 6509–6523, Jul. 26, 2021, doi: 10.1109/JLT.2021.3099009.

[19] R. J. Mailloux, *Phased Array Antenna Handbook* (Artech House antennas and propagation library), 2nd ed. Boston, MA, USA: Artech House, 2005.